

Two New Low Rank Tensor Completion Methods Based on Sum Nuclear Norm

Hongbing Zhang^a, Xinyi Liu^a, Hongtao Fan^{a,*}, Yajing Li^a, Yinlin Ye^a, Xinyun Zhu^b

^aCollege of Science, Northwest A&F University, Yangling, Shaanxi 712100, PR China

^bDepartment of Mathematics, University of Texas of the Permian Basin, Odessa, TX 79762, USA

Abstract

The low rank tensor completion (LRTC) problem has attracted great attention in computer vision and signal processing. How to acquire high quality image recovery effect is still an urgent task to be solved at present. This paper proposes a new tensor $L_{2,1}$ norm minimization model (TLNM) that integrates sum nuclear norm (SNN) method, differing from the classical tensor nuclear norm (TNN)-based tensor completion method, with $L_{2,1}$ norm and Qatar Riyal decomposition for solving the LRTC problem. To improve the utilization rate of the local prior information of the image, a total variation (TV) regularization term is introduced, resulting in a new class of tensor $L_{2,1}$ norm minimization with total variation model (TLNMTV). Both proposed models are convex and therefore have global optimal solutions. Moreover, we adopt the Alternating Direction Multiplier Method (ADMM) to obtain the closed-form solution of each variable, thus ensuring the feasibility of the algorithm. Numerical experiments show that the two proposed algorithms are convergent and outperform compared methods. In particular, our method significantly outperforms the contrastive methods when the sampling rate of hyperspectral images is 2.5%.

Keywords: Low rank tensor completion, sum nuclear norm (SNN) method, Qatar Riyal decomposition, $L_{2,1}$ norm, total variation, alternating direction multiplier method.

1. Introduction

The low rank tensor completion (LRTC) problem, especially when dealing with extremely high-dimensional data, such as appearing in color image and video processing [1], [2], magnetic resonance image [3], [4], hyperspectral image [5], [6], [7], pattern recognition [8], [9] face modeling and analysis [10] and other fields, has received extensive attention. The fact that the imaging of visual data is based on poor acquisition conditions or severe data corruption during transmission, results in incomplete or severely corrupted data being acquired. This will facilitate LRTC [11] to become crucially important

*Corresponding author

Email address: fanht17@nwafu.edu.cn (Hongtao Fan)

for collecting data, particularly how to utilize the internal structural information between collected observations and missing data to achieve LRTC problem.

Mathematically, the above LRTC problems can be characterized as follows:

$$\min_{\mathcal{X}} \quad \text{rank}(\mathcal{X}), \quad \text{s.t.} \quad \mathcal{X}_{\Omega} = \mathcal{T}_{\Omega} \quad (1)$$

where \mathcal{T} and \mathcal{X} represent the incomplete and complete tensors, respectively, Ω denotes an index set of observed data of \mathcal{T} , $\text{rank}(\mathcal{X})$ implies tensor rank of any tensor \mathcal{X} , conditions to be satisfied $\mathcal{X}_{\Omega} = \mathcal{T}_{\Omega}$ mean that the elements at the same positions in two sets \mathcal{X} and \mathcal{T} remain equal according to index set Ω .

It is well-known, on the one hand, that the definition of tensor rank is not unique, and its various definitions of tensor rank have been proposed according to different ways of tensor decomposition, such as CANDECOMP/PARAFAC(CP) rank [12], [13] generated by CP decomposition [14], Tucker-rank established by Tucker decomposition [15], [16], and tube rank and multi-rank based on tensor products [17], [18], etc. However, specific features, such as the calculation of the rank of a tensor CP is NP-hard [19], unfolding and folding of mode- n on a tensor in Tucker rank [20], [21] lead to dimensional disaster, and the limitation of the tensor product definition results in the multi-rank and tube rank [22], [23] based on t-SVD decomposition are only applicable to third-order tensors, indicate that the definitions of different tensor rank show their respective inadequacies. The other half is that tensor rank is a non-convex function.

In this regard, Liu et al. [24] turned to the convex envelope nuclear norm of the rank function to approximate it, and proposed a tensor nuclear norm minimization method to solve such problems, specifically, for image recovery problems

$$\min_{\mathcal{X}} \|\mathcal{X}\|_*, \quad \text{s.t.} \quad \mathcal{X}_{\Omega} = \mathcal{T}_{\Omega} \quad (2)$$

where $\|\mathcal{X}\|_* = \sum_{n=1}^N \alpha_n \|\mathbf{X}_{(n)}\|_*$ with $\alpha_n \geq 0$ and $\sum_{n=1}^N \alpha_n = 1$.

To further enhance, despite the model (2) has ideal effect in global information recovery, the performance of the model for local information extraction, especially in processing high-dimensional image recovery, by incorporating local piece-wise smoothness prior, and proposed a large class of Total Variation (TV) minimization methods [25] and applied to image processing and pattern recognition [16], [26], [27], [28]. In fact, for LRTC problems, TV terms are usually included in a low-rank (LR) framework to jointly represent local piecewise continuity and global LR structure along different dimensions [29], [30], [31], [32], which can greatly improve the local information effect of the model. Its specific modeling is as follows:

$$\min_{\mathcal{X}} \|\mathcal{X}\|_* + \lambda \|\mathcal{X}\|_{TV}, \quad s.t. \quad \mathcal{X}_\Omega = \mathcal{T}_\Omega \quad (3)$$

where $\|\mathcal{X}\|_{TV}$ is TV regularization term, and $\lambda > 0$ is a parameter used to balance the relationship between the nuclear norm and the regularization term.

Recently, Liu et al. [33] proposed an approximate SVD computation technique based on QR decomposition (CSVD-QR), and integrated $L_{2,1}$ norm to construct a fast and accurate matrix completion method. Inspired by the high performance of this method, Zheng et al. [34] designed a numerical method that approximates t-SVD combined with Qatari Riyal Decomposition (CTSVD-QR), which further generalizes the matrix-form QR method to the tensor case. Through in-depth comparative analysis and thorough experimental exploration, it is found that although the speed of the algorithm has been significantly improved, compared with the classical tensor nuclear norm (TNN) method, the performance of the algorithm in terms of image restoration effect or quality is still less ideal. In view of this, to improve and develop this method, we consider integrating tensor SNN, not TNN, with QR decomposition and $L_{2,1}$ norm to design and build a more efficient and feasible method, namely, tensor $L_{2,1}$ norm minimization model (TLNM). In order to further improve the effect of image restoration, that is, to better protect the local detail information while better representing the global information of the image, a TV regularization term is introduced and then a class of tensor $L_{2,1}$ norm minimizes the total variation model is proposed. To sum up, our main contributions are as follows:

Firstly, we adopt a new method different from TNN, that is, the integration of SNN and CSVD-QR method, to improve and enhance the restoration effect of the combination of LRTC and CSVD-QR method. For the sake of fairness, we still choose the $L_{2,1}$ norm instead of the classical nuclear norm in the objective function as in the recently published papers [33] and [34]. In the meantime, by introducing the TV regularization term into the model constructed above, a new method named tensor $L_{2,1}$ norm minimization with TV (TLNMTV) is established to better preserve some details of the image, thereby improving the utilization of the local prior information of the image.

Secondly, for the above two established LRTC models, namely TLNM and TLMNTV, two efficient alternating direction multiplier (ADMM) algorithms [35], [36] are designed to solve them respectively. The closed-form solution of each variable can be obtained by the ADMM algorithm, so that the algorithm can be effectively implemented, thus maintaining the accuracy. Furthermore, the experimental results show that the relative error (RE) of these two algorithms always decreases, hence ensuring that they are indeed convergent.

Thirdly, extensive real-data experiments show that the TLNM method obviously outperforms the classical TNN method, which indicates that our proposed integrating QR decomposition and SNN method outperforms the TNN-based TLNM-TQR [34] method. More importantly, the TLMNTV

method further enhances the local sparsity, with higher quantitative numerical result and better visual restoration effect than other comparison methods in this paper. It is also particularly worth mentioning that when the sampling rate of hyperspectral images is 2.5%, our methods can perform image restoration clearly and very well and are shown to be the best.

2. PRELIMINARIES

We are now in a position to give the basic notation of the tensors involved and lay out the basic definitions and theorems for constructing the two proposed new methods.

2.1. Tensor Notations and their Definitions

Generally, the uppercase and lowercase of any letter represent respectively vectors and matrices, such as x represents a vector and X represents a matrix. We use a calligraphic upper case letter $\mathcal{X} \in \mathbb{R}^{I_1 \times I_2 \times \dots \times I_N}$ to represent an N th-order tensor, and x_{i_1, i_2, \dots, i_N} to represent its (i_1, i_2, \dots, i_N) -th element. Unless otherwise stated, we still use $\|\mathcal{X}\|_F = (\sum_{i_1, i_2, \dots, i_N} x_{i_1, i_2, \dots, i_N}^2)^{1/2}$ as the definition of the Frobenius norm and define the inner product of two N th-order tensors \mathcal{Y} and \mathcal{Z} as $\langle \mathcal{Y}, \mathcal{Z} \rangle = \sum_{i_1, i_2, \dots, i_N} y_{i_1, i_2, \dots, i_N} z_{i_1, i_2, \dots, i_N}$, where y_{i_1, i_2, \dots, i_N} and z_{i_1, i_2, \dots, i_N} stand for the (i_1, i_2, \dots, i_N) -th element of \mathcal{Y} and \mathcal{Z} , respectively.

Definition 1 ([37]). The mode- n unfolding of a tensor $\mathcal{X} \in \mathbb{R}^{I_1 \times I_2 \times \dots \times I_N}$ is denoted as a matrix $\mathbf{X}_{(n)} \in \mathbb{R}^{I_n \times I_1 \dots I_{n-1} I_{n+1} \dots I_N}$. Tensor element (i_1, i_2, \dots, i_N) maps to matrix element (i_n, j) , where

$$j = 1 + \sum_{k=1, k \neq n}^N (i_k - 1) J_k \quad \text{with} \quad J_k = \prod_{m=1, m \neq n}^{k-1} I_m. \quad (4)$$

The mode- n unfolding operator and its corresponding inverse operator are abbreviated as unfold_n and fold_n , and satisfy transformation relation $\mathcal{X} = \text{fold}_n(\mathbf{X}_{(n)}) = \text{fold}_n(\text{unfold}_n(\mathcal{X}))$.

Definition 2 ([37]). The mode- n product operation between tensor $\mathcal{X} \in \mathbb{R}^{I_1 \times I_2 \times \dots \times I_N}$ and matrix $U \in \mathbb{R}^{J_n \times I_n}$ is expressed as $\mathcal{Y} = \mathcal{X} \times_n U$, where $\mathcal{Y} \in \mathbb{R}^{I_1 \times I_2 \times \dots \times I_{n-1} J_n I_{n+1} \dots I_N}$. Elementwisely, we have

$$\mathcal{Y} = \mathcal{X} \times_n U \quad \Leftrightarrow \quad \mathbf{Y}_{(n)} = U \cdot \text{unfold}_n(\mathbf{X}_{(n)}). \quad (5)$$

Definition 3 ([38]). The $L_{2,1}$ norm of a matrix $M \in \mathbb{R}^{I \times J}$ can be defined as

$$\|M\|_{2,1} = \sum_{j=1}^J \sqrt{\sum_{i=1}^I m_{ij}^2}, \quad (6)$$

where $m_{i,j}$ represents the element at row i -th and column j -th of the matrix M .

Algorithm 1 CSVD-QR[33]

Input: X , a real matrix $C \in \mathbb{R}^{m \times n}$; $It_{max} > 0$

Initialization: $r > 0$, $q > 0$, $k = 1$; ε is a positive tolerance, $L_0 = eye(m, r)$, $D_0 = eye(r, r)$, $R_0 = eye(r, n)$.

while $\|L_k D_k R_k - X\| \geq \varepsilon$ or $k < It_{max}$ **do**

$[Q, T] = qr(X R_k^T)$;

$L_{k+1} = Q(:, 1 : r)$.

$[Q, T] = qr(X^T L_{j+1})$;

$R_{k+1} = Q(:, 1 : r)^T$.

$D_{k+1} = T(1 : r, 1 : r)^T$.

$k = k + 1$.

end while

return $L = L_k$, $D = D_k$, $R = R_k$

Output: L , D , R ($X = LDR$)

The $L_{2,1}$ norm has been successfully applied to low-rank representation [38] to optimize the noise data matrix $K \in \mathbb{R}^{m \times n}$, which can be updated by solving the minimization problem as follows:

$$\min_K \tau \|K\|_{2,1} + \frac{1}{2} \|K - C\|_F^2, \quad (7)$$

where $C \in \mathbb{R}^{m \times n}$ is a pre-determined real matrix and $\tau > 0$.

Here we will describe an approximate SVD (CSVD-QR) method based on QR decomposition mainly used in this paper, see [33], and the corresponding CSVD-QR algorithm can be specifically shown in Algorithm 1 below.

Theorem 1 ($L_{2,1}$ norm minimization solver (LNMS) [33]). *The optimal $K(:, j)$, i.e., the j th column of K , of the problem in (7) follows*

$$K(:, j) = \frac{\max\{\|C(:, j)\|_2 - \tau, 0\}}{\|C(:, j)\|_2} C(:, j), \quad (8)$$

where $\|C(:, j)\|_2 = \sqrt{\sum_{i=1}^m C_{ij}^2}$.

3. Models and Algorithms

3.1. Tensor $L_{2,1}$ Norm Minimization Model With Its Algorithm

For LRTC problem, to further improve the quality and visual effect of image restoration, we integrate the $L_{2,1}$ norm and CSVD-QR method into the tensor SNN minimization problem instead of the classical tensor TNN method, resulting in a tensor $L_{2,1}$ norm minimization model as below:

$$\begin{aligned}
& \min_{\mathcal{X}} \sum_{n=1}^N \alpha_n \|D_n\|_{2,1} \\
& s.t. \quad \{\mathcal{M}_n = \mathcal{X}\}_{n=1}^N, \quad \{\mathbf{M}_{n(n)} = L_n D_n R_n\}_{n=1}^N, \\
& \quad \mathcal{X}_\Omega = \mathcal{T}_\Omega, \quad L_n^T L_n = I_n, \quad R_n R_n^T = I_n,
\end{aligned} \tag{9}$$

where $\mathcal{M}_n, n = 1, 2, \dots, N$ indicate auxiliary parameters, $\sum_{n=1}^N \alpha_n = 1$, L_n, D_n, R_n are induced by $\mathbf{M}_{n(n)}$ when completing CSVD-QR decomposition, Ω represents the exact locations of known observations. It is worth mentioning here that we still adopt the $L_{2,1}$ norm accommodating with CSVD-QR method and the tensor SNN minimization method to replace the nuclear norm in the objective function, which exactly shows the novelty and superiority of proposed method compared with the existing state-of-the-art methods and ensures the fairness in performing trial comparisons between two recently published methods [33] and [34].

3.2. Optimization TLNM Algorithm Based on ADMM

With the augmented Lagrangian formula, the above model (9) can be transformed into the following optimization form:

$$\begin{aligned}
& Lag(\mathcal{X}, \{\mathcal{M}_n, \mathcal{Q}_n, L_n, R_n, D_n, \Phi_n\}_{n=1}^N) \\
& = \sum_{n=1}^N \alpha_n \|D_n\|_{2,1} + \frac{\mu}{2} \|\mathbf{M}_{n(n)} - L_n D_n R_n + \frac{\Phi_n}{\mu}\|_F^2 \\
& + \frac{\mu}{2} \|\mathcal{M}_n - \mathcal{X} + \frac{\mathcal{Q}_n}{\mu}\|_F^2,
\end{aligned} \tag{10}$$

where matrices \mathcal{Q}_n and Φ_n denote the Lagrange multipliers and $\mu > 0$. Now, we start to optimize the problem (10) under the ADMM framework. Here we use these matrix symbols $L_n^+, R_n^+, D_n^+, \mathcal{M}_n^+, \mathcal{X}^+$ to represent the final results of iterative updates in ADMM respectively.

3.2.1. Optimize $\{L_1, \dots, L_N\}$

Let the initial values of all parameter matrices L_n, D_n, R_n in the proposed algorithm be $L_n^0 = eye(I_n, r_n)$, $D_n^0 = eye(r_n, r_n)$, $R_n^0 = eye(r, t_n)$ and $t_n = I_1 \cdots I_{n-1} I_{n+1} \cdots I_N$, respectively, where *eye* is the built-in command for the identity matrix in MATLAB. Keep other variables unchanged in (10), the optimization objective function with respect to L_n becomes

$$\min_{L_n, R_n} \|\mathbf{M}_{n(n)} - L_n D_n R_n + \frac{\Phi_n}{\mu}\|_F^2. \tag{11}$$

Here, we regard the solution of problem (11) as the iterative solution process of the CSVD-QR method based on matrix $\mathbf{M}_{n(n)} + \frac{\Phi_n}{\mu}$, which can be accurately expressed as follows:

$$\mathbf{M}_{n(n)} + \frac{\Phi_n}{\mu} = L_n D_{Tn} R_n, \tag{12}$$

where $D_{Tn} \in \mathbb{R}^{r_n \times r_n}$. If we let $\mathbf{M}_{n(n)}^k + \frac{\Phi_n^k}{\mu} = G_n$, then L_n^{k+1} can be obtained recursively as follows:

$$[Q, T] = qr(G_n R_n^T) \quad (13)$$

$$L_n^+ = Q(q_1, \dots, q_{r_n}) \quad (14)$$

where matrices $Q \in \mathbb{R}^{I_n \times I_n}$ and $T \in \mathbb{R}^{I_n \times r_n}$ are treated as intermediate variables.

3.2.2. Optimize $\{R_1, \dots, R_N\}$

In a similar manner, R_n^{k+1} can be derived iteratively as follows:

$$[Q, T] = qr(G_n^T L_n) \quad (15)$$

$$R_n^+ = Q(q_1, \dots, q_{r_n})^T \quad (16)$$

where $Q \in \mathbb{R}^{t_n \times t_n}$ and $T \in \mathbb{R}^{t_n \times r_n}$ are considered as intermediate variables.

3.2.3. Optimize $\{D_1, \dots, D_N\}$

With $\mathbf{M}_{n(n)}$, Φ_n , L_n , and R_n held fixed, the variable D_n can be optimally solved in the following way:

$$D_n = \arg \min_{D_n} \frac{\alpha_n}{\mu} \|D_n\|_{2,1} + \frac{1}{2} \|D_n - L_n^T(\mathbf{M}_{n(n)} + \frac{\Phi_n}{\mu}) R_n^T\|_F^2. \quad (17)$$

Combine (12) with (17), we get:

$$D_{Rn} = L_n^T(\mathbf{M}_{n(n)} + \frac{\Phi_n}{\mu}) R_n^T \quad (18)$$

As a result, (17) can be equivalently expressed as:

$$D_n = \arg \min_{D_n} \frac{\alpha_n}{\mu} \|D_n\|_{2,1} + \frac{1}{2} \|D_n - D_{Rn}\|_F^2. \quad (19)$$

With the result of Theorem 1, we can approximate and update D_n through the following formula:

$$D_n^+ = D_{Rn} G_n, \quad (20)$$

where

$$G_n = \text{diag}(g_{n1}, \dots, g_{nr_n}), \quad (21)$$

and the j th entry g_{nj} can be calculated by using the following formula:

$$g_{nj} = \frac{\max\{\|D_{Rn}(:, j)\|_F - \frac{\alpha_n}{\mu}, 0\}}{\|D_{Rn}(:, j)\|_F}. \quad (22)$$

Algorithm 2 TLNM

Input: any incomplete tensor \mathcal{T} , the index set representing the position of known tensor elements Ω , convergence criteria ϵ , prescribed iteration number K .

Initialization: $\mathcal{X}^0 = \mathcal{T}_\Omega$, $\{\mathcal{M}_n^0 = \mathcal{X}^0\}_{n=1}^N$, $\mu^0 > 0$, $\rho > 1$, $\{\alpha_n, r_n, L_n^0, D_n^0, R_n^0\}_{n=1}^N$.

```
1: while not converged and  $k < K$  do
2:   for  $n=1:N$  do
3:     Compute  $L_n^k$  via (13-14);
4:     Compute  $R_n^k$  via (15-16);
5:     Compute  $D_n^k$  via (20);
6:     Compute  $\mathcal{M}_n^k$  via (25);
7:   end for
8:   Compute  $\mathcal{X}^k$  via (26);
9:   Compute the multipliers  $\mathcal{Q}_n^k$  and  $\Phi_n^k$  via (27);
10:   $\mu^k = \rho\mu^{k-1}$ ,  $k = k + 1$ ;
11:  Check whether the convergence condition  $\|\mathcal{X}^{k+1} - \mathcal{X}^k\|_\infty \leq \epsilon$  is satisfied
12: end while
13: return  $\mathcal{X}^{k+1}$ 
```

Output: Completed tensor $\mathcal{X} = \mathcal{X}^{k+1}$

3.2.4. Optimize $\{\mathcal{M}_1, \dots, \mathcal{M}_N\}$

Under the assumption that other variables remain unchanged, the optimization objective function with respect to \mathcal{M}_n can degenerate into

$$\begin{aligned} \mathcal{M}_n = \min_{\mathcal{M}_n} & \|\mathbf{M}_{n(n)} - L_n D_n R_n + \frac{\Phi_n}{\mu}\|_F^2 \\ & + \|\mathcal{M}_n - \mathcal{X} + \frac{\mathcal{Q}_n}{\mu}\|_F^2. \end{aligned} \quad (23)$$

Using the definitions and properties of tensor (matrix) Frobenius norm, \mathcal{M}_n of (23) can be equivalently reformulated as

$$\begin{aligned} \mathbf{M}_{n(n)} = \min_{\mathcal{M}_n} & \|\mathbf{M}_{n(n)} - L_n D_n R_n + \frac{\Phi_n}{\mu}\|_F^2 \\ & + \|\mathbf{M}_{n(n)} - \mathbf{X}_{(n)} + \frac{\mathbf{Q}_{n(n)}}{\mu}\|_F^2. \end{aligned} \quad (24)$$

Accordingly, \mathcal{M}_n^+ is deduced as follows:

$$\mathcal{M}_n^+ = fold_n\left(\frac{1}{2}(\mathbf{X}_{(n)} - \frac{\mathbf{Q}_{n(n)}}{\mu} + L_n D_n R_n - \frac{\Phi_n}{\mu})\right). \quad (25)$$

3.2.5. Optimize \mathcal{X}

The optimal solution for the variable \mathcal{X} can be obtained by optimizing the minimization function of the following problem:

$$\mathcal{X}^+ = \min_{\mathcal{X}} \sum_{n=1}^N \frac{\mu}{2} \|\mathcal{M}_n - \mathcal{X} + \frac{\mathcal{Q}_n}{\mu}\|_F^2 \quad s.t. \quad \mathcal{X}_\Omega = \mathcal{T}_\Omega.$$

its specific explicit closed-form solution can be written as

$$\begin{cases} \mathcal{X}_\Omega^+ = \mathcal{T}_\Omega, \\ \mathcal{X}_{\Omega^\perp}^+ = \frac{1}{N\mu} (\sum_{n=1}^N \mu \mathcal{M}_n + \mathcal{Q}_n)_{\Omega^\perp}, \end{cases} \quad (26)$$

where the vertical symbol $^\perp$ in the upper right corner of Ω indicates the complement set Ω^\perp of Ω .

3.2.6. Update the multipliers \mathcal{Q}_n, Φ_n

$$\begin{cases} \mathcal{Q}_n^+ = \mathcal{Q}_n + \mu(\mathcal{M}_n - \mathcal{X}), \\ \Phi_n^+ = \Phi_n + \mu(\mathbf{M}_{n(n)} - L_n D_n R_n), \\ \mu^+ = \rho\mu, \end{cases} \quad (27)$$

where $\rho \geq 1$.

So far, all the above variables have been updated and solved, and the pseudocode corresponding to all algorithms for TLNM has been reported in detail in Algorithm 2.

3.3. Tensor $L_{2,1}$ -Norm Minimization with Total variation (TLNMTV)

Total variation method is inherently remarkable in the protection of image details so as to improve the utilization rate of the local prior information of the image. In this regard, we investigate and propose the tensor $L_{2,1}$ norm minimization with TV (TLNMTV) method to obtain the following model by adding the regularization term of the form in [31].

$$\min_{\mathcal{X}} \sum_{n=1}^N \alpha_n \|\mathbf{X}_{(n)}\|_* + \lambda \sum_{n=1}^N \beta_n |C_n \mathbf{X}_{(n)}| \quad s.t. \quad \mathcal{X}_\Omega = \mathcal{T}_\Omega. \quad (28)$$

Here, the latter term is the TV regularization term, where the dimension of C_n is $(I_n - 1, I_n)$ with $(C_n)_{i,i} = 1$ and $(C_n)_{i,i+1} = -1$. The operator $|\cdot|$ of any matrix X is defined as $|X| = \sum_{i=1} \sum_{j=1} |X_{i,j}|$. The parameter λ is represented as a tunable hyperparameter. These parameters β_1, \dots, β_N take either the value 0 or 1, which means whether the smoothing and piecewise prior information on the n -th mode of the completed tensor is known or not. However, as we know, different dimensions of different high-dimensional data represent different data information, and some information is not smooth. For this, it is not necessary to compute smoothing and piecewise priors in this dimension. It should be pointed

out that, quite different from the traditional regular meaning, the TV term used here is only able to determine whether smoothing and piecewise priors need to be computed for different modes. Therefore, it is more reasonable to use the TV regularization term in combination with the actual situation. In particular, when the TV regularization term is removed, the problem degenerates itself into a low-rank tensor problem (2).

In this connection, by introducing auxiliary matrix and tensor variable sets $\{Q_n\}_{n=1}^N$, $\{A_n\}_{n=1}^N$, $\{Z_n\}_{n=1}^N$ for these variables $\mathbf{X}_{(n)}$, $C_n A_n$ and \mathcal{X} , respectively, i.e., $A_n = \mathbf{X}_{(n)}$, $Q_n = C_n A_n$ and $Z_n = \mathcal{X}$, the proposed tensor $L_{2,1}$ -norm minimization with TV model (TLNMTV) can be induced as follows:

$$\begin{aligned} \min_{\mathcal{X}} \quad & \sum_{n=1}^N \alpha_n \|D_n\|_{2,1} + \lambda \sum_{n=1}^N \beta_n |Q_n| \\ \text{s.t.} \quad & \mathcal{X}_\Omega = \mathcal{T}_\Omega, \{Q_n = C_n A_n, Z_n = \mathcal{X}, A_n = \mathbf{X}_{(n)}\}_{n=1}^N, \\ & \{\mathbf{Z}_{n(n)} = L_n D_n R_n\}_{n=1}^N, L_n^T L_n = I_n, R_n R_n^T = I_n. \end{aligned} \quad (29)$$

Due to the fact that this model (29) is convex we can solve it using the ADMM framework.

3.4. Optimization TLNMTV Algorithm Based on ADMM

With the augmented Lagrange thinking, the optimization problem (29) can be transformed into:

$$\begin{aligned} \text{Lag}(\mathcal{X}, \{Z_n, \mathcal{G}_n, Q_n, \Lambda_n, A_n, \Gamma_n, L_n, R_n, D_n, \Phi_n\}_{n=1}^N) \\ = \sum_{n=1}^N (\alpha_n \|D_n\|_{2,1} + \frac{\mu}{2} \|Z_n - \mathcal{X} + \frac{\mathcal{G}_n}{\mu}\|_F^2) \\ + \sum_{n=1}^N \beta_n (\lambda |Q_n| + \frac{\mu}{2} \|Q_n - C_n A_n + \frac{\Lambda_n}{\mu}\|_F^2) \\ + \sum_{n=1}^N \beta_n (\frac{\mu}{2} \|A_n - \mathbf{X}_{(n)} + \frac{\Gamma_n}{\mu}\|_F^2) \\ + \sum_{n=1}^N \frac{\mu}{2} \|\mathbf{Z}_{n(n)} - L_n D_n R_n + \frac{\Phi_n}{\mu}\|_F^2, \end{aligned} \quad (30)$$

where matrices $\{\Lambda_n\}_{n=1}^N$, $\{\Gamma_n\}_{n=1}^N$, $\{\Phi_n\}_{n=1}^N$ and tensors $\{\mathcal{G}_n\}_{n=1}^N$ represent, respectively, Lagrange multipliers, $\mu > 0$. Next, we explicitly give their respective formulas for these optimization variables $\{Q_n\}_{n=1}^N$, $\{L_n\}_{n=1}^N$, $\{R_n\}_{n=1}^N$, $\{D_n\}_{n=1}^N$, $\{Z_n\}_{n=1}^N$, $\{A_n\}_{n=1}^N$ and \mathcal{X} .

3.4.1. Optimize $\{Q_1, \dots, Q_N\}$

Under the premise of ensuring that other variables do not change, we can transform the optimization problem of $\{Q_1, \dots, Q_N\}$ into a form of:

$$\min_{\{Q_1, \dots, Q_N\}} \sum_{n=1}^N \beta_n (\lambda |Q_n| + \frac{\mu}{2} \|Q_n - C_n A_n + \frac{\Lambda_n^k}{\mu}\|_F^2). \quad (31)$$

Based on the fact that the matrix groups $\{Q_1, \dots, Q_N\}$ in the optimization problem are independent of each other, the solution formula for each of them can be easily obtained:

$$Q_n = \beta_n \cdot shrinkage_{\frac{\Delta}{\mu}}(C_n A_n - \frac{1}{\mu} \Lambda_n), \quad (32)$$

where the operator symbol $shrinkage_{\alpha}(\cdot)$ represents the elementwise shrinkage thresholding operator of a matrix, i.e.,

$$shrinkage_{\alpha}(X)_{i,j} = (X)_{i,j} - \min(\alpha, |(X)_{i,j}|) \cdot \frac{(X)_{i,j}}{|(X)_{i,j}|},$$

and $\frac{(X)_{i,j}}{|(X)_{i,j}|}$ is equal to zero when $(X)_{i,j} = 0$.

3.4.2. Optimize $\{L_1, \dots, L_N\}, \{R_1, \dots, R_N\}, \{D_1, \dots, D_N\}$

Since the update of these variables L_1, \dots, L_N , R_1, \dots, R_N and D_1, \dots, D_N is consistent with the TLNM algorithm, it is omitted here and will not be repeated.

3.4.3. Optimize $\{\mathcal{Z}_1, \dots, \mathcal{Z}_N\}$

By keeping the rest of the variables unchanged, the optimization problem with respect to \mathcal{Z}_n can be precisely described as below

$$\mathcal{Z}_n = \min_{\mathcal{Z}_n} \|\mathbf{Z}_{n(n)} - L_n D_n R_n + \frac{\Phi_n}{\mu}\|_F^2 + \|\mathcal{Z}_n - \mathcal{X} + \frac{\mathcal{Q}_n}{\mu}\|_F^2. \quad (33)$$

With the help of the definition of tensor Frobenius norm and matrix Frobenius norm, the above problem (33) can be equivalently transformed into

$$\mathbf{Z}_{n(n)} = \min_{\mathcal{Z}_n} \|2\mathbf{Z}_{n(n)} - L_n D_n R_n + \frac{\Phi_n}{\mu} - \mathbf{X}_{(n)} + \frac{\mathbf{Q}_{n(n)}}{\mu}\|_F^2. \quad (34)$$

Therefore \mathcal{Z}_n^+ is obtained as follows:

$$\mathcal{Z}_n^+ = fold_n(\frac{1}{2\mu}(\mu\mathbf{X}_{(n)} - \mathbf{Q}_{n(n)} + \mu L_n D_n R_n - \Phi_n)). \quad (35)$$

3.4.4. Optimize $\{A_1, \dots, A_N\}$

Make sure that the rest of the above variables do not change, we can reformulate the above optimization problem of $\{A_1, \dots, A_N\}$ into the following form:

$$\min \sum_{n=1}^N (\|Q_n - C_n A_n + \frac{\Lambda_n}{\mu}\|_F^2 + \|A_n - \mathbf{X}_{(n)} + \frac{\Gamma_n}{\mu}\|_F^2). \quad (36)$$

This type of problem (36) can be solved by dividing it into N sub-problems, each of which can be expressed in this form:

$$A_n = \arg \min_{A_n} \|Q_n - C_n A_n + \frac{\Lambda_n}{\mu}\|_F^2 + \|A_n - \mathbf{X}_{(n)} + \frac{\Gamma_n}{\mu}\|_F^2. \quad (37)$$

In this regard, by solving the above minimization problem, the following update formula is derived:

$$A_n^+ = (\mu C_n^T C_n + \mu I)^{-1} (C_n^T \Lambda_n + \mu C_n^T Q_n + \mu \mathbf{X}_{(n)} - \Gamma_n), \quad (38)$$

where I is the identity matrix of the appropriate order.

3.4.5. Optimize \mathcal{X}

We obtain the variable \mathcal{X} by solving the following constraint minimization function:

$$\begin{aligned} \mathcal{X} = \min_{\mathcal{X}} \sum_{n=1}^N (\|\mathcal{Z}_n - \mathcal{X} + \frac{\mathcal{G}_n}{\mu}\|_F^2 + \beta_n \|A_n - \mathbf{X}_{(n)} + \frac{\Gamma_n}{\mu}\|_F^2) \\ \text{s.t. } \mathcal{X}_\Omega = \mathcal{T}_\Omega, \end{aligned} \quad (39)$$

whose closed-form solution can be expressed as

$$\begin{cases} \mathcal{X}_\Omega^+ = \mathcal{T}_\Omega, \\ \mathcal{X}_{\Omega^\perp}^+ = \frac{[\sum_{n=1}^N \mu \mathcal{Z}_n + \mathcal{G}_n + \text{fold}_n(\mu A_n + \Gamma_n)]_{\Omega^\perp}}{(N + \sum_{n=1}^N \beta_n) \mu}. \end{cases} \quad (40)$$

3.4.6. Update the multipliers \mathcal{G}_n , Λ_n , Φ_n and Γ_n

$$\begin{cases} \mathcal{G}_n^+ = \mathcal{G}_n + \mu(\mathcal{Z}_n - \mathcal{X}), \\ \Lambda_n^+ = \Lambda_n + \mu(Q_n - C_n A_n), \\ \Gamma_n^+ = \Gamma_n + \mu(A_n - \mathbf{X}_{(n)}), \\ \Phi_n^+ = \Phi_n + \mu(\mathbf{Z}_{n(n)} - L_n D_n R_n), \end{cases} \quad (41)$$

and $\mu^+ = \rho\mu$, where $\rho \geq 1$. The pseudo-code corresponding to our proposed algorithm for TLNMTV is displayed in the table, i.e., Algorithm 3.

3.5. Computational Complexity Analysis of Corresponding Algorithms

For any input tensor $\mathcal{T} \in \mathbb{R}^{I_1 \times I_2 \times \dots \times I_N}$ of size N -order, the entire computational complexity of Algorithm 2 includes the following five major aspects.

Updating the matrix L_n needs to give the decomposition of QR [see (13)-(14)], and the complexity of which is $O(I_n r_n^2)$, and the total computational complexity of these variable matrices $L_n (n = 1, 2, \dots, N)$ is $O(\sum_{n=1}^N I_n r_n^2)$.

Likewise, the complexity of calculating R_n is $O(\sum_{n=1}^N r_n^2 \prod_{i=1, i \neq n}^N I_i)$.

When updating matrix D_n , it is necessary to perform the product operation between two $r_n \times r_n$ matrices for solving the LNMS problem, thus the computational complexity of all these variable matrices $D_n (n = 1, 2, \dots, N)$ is $O(\sum_{n=1}^N r_n^2)$.

Algorithm 3 TLNMTV

Input: an arbitrary incomplete tensor \mathcal{T} , the set of indices of the known elements Ω , convergence stop criteria ϵ , maximum number of iteration steps K .

Initialization: $\mathcal{X}^0 = \mathcal{T}_\Omega$, $\{\mathcal{Z}_n^0 = \mathcal{X}^0\}_{n=1}^N$, $\mu^0 > 0$, $\rho > 1$, $\{\alpha_n, r_n, L_n^0, D_n^0, R_n^0\}_{n=1}^N$.

```
1: while not converged and  $k < K$  do
2:   for  $n=1:N$  do
3:     Calculate  $Q_n^k$  via (32);
4:     Calculate  $L_n^k$  via (13-14);
5:     Calculate  $R_n^k$  via (15-16);
6:     Calculate  $D_n^k$  via (20);
7:     Calculate  $\mathcal{Z}_n^k$  via (35);
8:     Calculate  $A_n^k$  via (38);
9:   end for
10:  Calculate  $\mathcal{X}^k$  via (40);
11:  Calculate the multipliers  $\mathcal{G}_n$ ,  $\Lambda_n$ ,  $\Phi_n$ , and  $\Gamma_n$  via (41);
12:   $\mu^{k+1} = \rho\mu^k$ ,  $k = k + 1$ ;
13:  Check whether the convergence condition  $\|\mathcal{X}^{k+1} - \mathcal{X}^k\|_\infty \leq \epsilon$  is satisfied
14: end while
15: return  $\mathcal{X}^{k+1}$ 
```

Output: Completed tensor $\mathcal{X} = \mathcal{X}^{k+1}$

Updating each matrix \mathcal{M}_n requires the product operation of these three matrices L_n , D_n , and R_n in advance, for which the computational complexity of all the corresponding variable matrices $\mathcal{M}_n (n = 1, 2, \dots, N)$ is $O(\sum_{n=1}^N (I_n r_n^2 + r \prod_{i=1}^N I_i))$.

In addition, the complexity of updating matrix \mathcal{X} is known as $O(\prod_n I_n)$. Thus, by summing the above complexities, all the computational complexity of Algorithm 2 is $O(K(\sum_{n=1}^N (I_n r_n^2 + r_n^2 \prod_{i=1, i \neq n}^N I_i + r_n^2 + I_n r_n^2 + r \prod_{i=1}^N I_i) + \prod_n I_n))$.

Similarly, the entire computational complexity of Algorithm 3 is mainly composed of the following seven parts.

It is easy to know that the computational complexity required to update the matrix Q_n is $O(\sum_{n=1}^N (I_n - 1) \prod_n I_n)$.

The computational complexity required to update these matrices L_n , R_n , D_n is the same as in Algorithm 2.

Updating \mathcal{Z}_n requires calculating the product of the three matrices $L_n D_n R_n$ in advance, the complexity of these variable matrices $\mathcal{Z}_n (n = 1, 2, \dots, N)$ is $O(\sum_{n=1}^N (I_n r_n^2 + r \prod_{i=1}^N I_i))$.

Updating A_n requires calculating the inverse of a matrix of order $I_n \times I_n$ and the product matrix of any matrix, the complexity of which is $O(I_n^3 + I_n^2 \prod_{i=1, i \neq n}^N I_i)$. The complexity of these variable matrices $A_n (n = 1, 2, \dots, N)$ is $O(\sum_{n=1}^N I_n^3 + I_n^2 \prod_{i=1, i \neq n}^N I_i)$

The computational complexity required to update a tensor \mathcal{X} is $O(\prod_n I_n)$. Thus, the total computational complexity of our proposed Algorithm 3 is $O(K(\sum_{n=1}^N ((I_n - 1) \prod_n I_n + I_n r_n^2 + r_n^2 \prod_{i=1, i \neq n}^N I_i + r_n^2 + I_n r_n^2 + r \prod_{i=1}^N I_i + I_n^3 + I_n^2 \prod_{i=1, i \neq n}^N I_i) + \prod_n I_n))$.

4. Experiments

In this section, two typical tensor data, i.e., HSI data and MRI data are employed to illustrate the performance of the proposed method. Four quantitative picture quality indices (PQIs) are used to evaluate the quality of recovery, including peak signal-to-noise ratio (PSNR), structural similarity (SSIM) [39] feature similarity (FSIM) [40], and erreur relative globale adimensionnelle de synthèse (ERGAS) [41]. All tests are implemented on the Windows 10 platform and MATLAB (R2019a) with an Intel Core i7-10875H 2.30 GHz and 32 GB of RAM.

We compare our results with nine recently developed state-of-the-art LRTC methods, including the tensor trace norm-based LRTC (HaLRTC) [24], the t-SVD-based TC method [42], alternating direction multiplier method(ADM)-based matrix completion (MC-ALM) [43], the nonconvex tensor rank constraint-based, i.e., the minimax concave plus penalty-based TC (McpTC) and the smoothly clipped absolute deviation penalty-based TC (ScadTC) method [44], the parallel matrix factorization-based LRTC method (TMac) [30], the LRTC with TV on tensor unfolding (LRTC-TV) [31], Tensor Completion based Framelet Representation of Tensor Nuclear Norm(FTNN)[45], and the joint trace/TV-based TC method (Trace/TV) [46]. All comparison methods use the corresponding optimal parameters for the experiment.

Table 1: Average quantitative evaluation of the results for HSIs with different SRs.

SR	index	Observed	MC-ALM	HaLRTC	Tmac	LRTC-TV	Trace-TV	t-SVD	McpTC	ScadTC	FTNN	TLNM	TLNMTV
5%	PSNR	14.169	23.438	22.995	14.212	24.257	18.660	27.680	28.739	28.560	27.237	31.136	32.666
	SSIM	0.203	0.593	0.650	0.226	0.709	0.621	0.727	0.725	0.701	0.763	0.790	0.857
	FSIM	0.644	0.797	0.777	0.658	0.796	0.775	0.898	0.888	0.886	0.882	0.936	0.959
	ERGAS	910.569	332.274	350.889	906.147	308.510	562.121	210.364	195.615	199.534	221.914	139.178	116.057
10%	PSNR	14.403	25.976	26.303	14.486	27.901	26.580	31.374	31.936	31.881	31.614	33.787	35.632
	SSIM	0.238	0.694	0.745	0.269	0.817	0.812	0.841	0.823	0.811	0.876	0.858	0.910
	FSIM	0.688	0.861	0.856	0.696	0.894	0.919	0.949	0.937	0.935	0.950	0.964	0.979
	ERGAS	886.354	252.090	246.122	878.174	204.648	247.447	139.290	134.702	137.803	134.651	105.123	85.385
20%	PSNR	14.915	29.336	30.575	15.262	35.053	35.053	36.054	35.728	35.705	37.290	36.500	38.578
	SSIM	0.303	0.811	0.859	0.348	0.945	0.945	0.927	0.911	0.900	0.955	0.916	0.952
	FSIM	0.734	0.924	0.936	0.744	0.984	0.984	0.980	0.973	0.971	0.986	0.983	0.989
	ERGAS	835.570	173.900	152.819	805.944	93.710	93.710	83.575	86.751	89.127	71.704	78.446	62.725

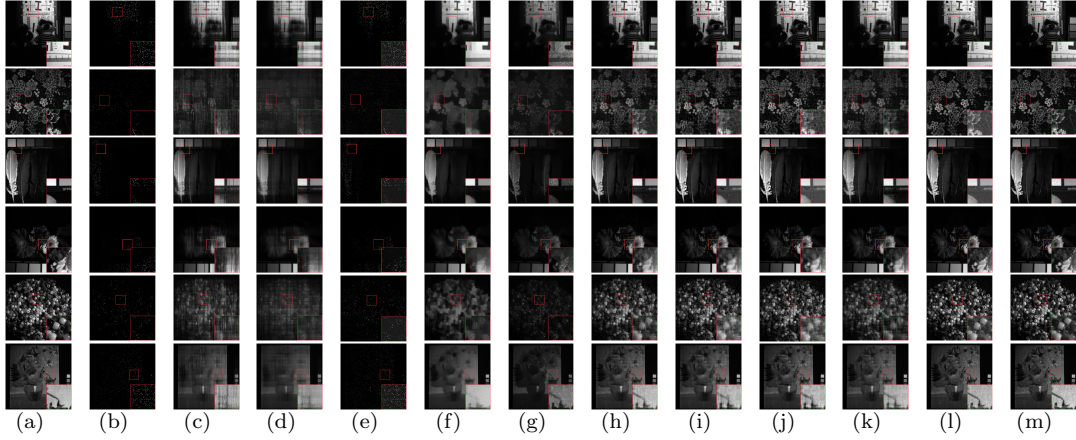


Figure 1: (a) Original images. (b) Corresponding sampled images with SR 5%. (c)-(l) and (m) Completed images achieved by nine competing methods and proposed TLNM method and TLNMTV method, respectively. (a) Original image. (b) Observed image. (c) MC-ALM. (d) HaLRTC. (e) TMac. (f) LRTC-TV. (g) Trace/TV. (h) t-SVD. (i) McpTC. (j) ScadTC. (k) FTNN. (l) TLNM. (m) TLNMTV.

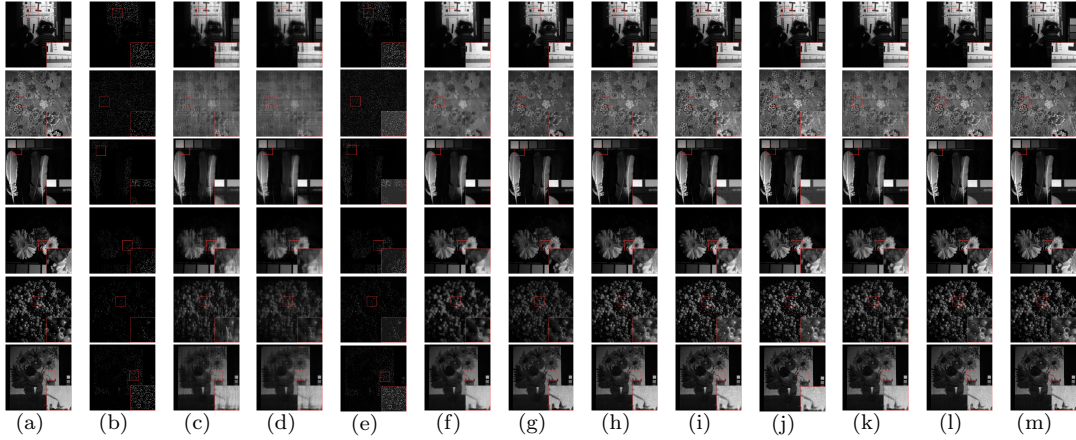


Figure 2: (a) Original images. (b) Corresponding sampled images with SR 10%. (c)-(l) and (m) Completed images achieved by nine competing methods and proposed TLNM method and TLNMTV method, respectively. (a) Original image. (b) Observed image. (c) MC-ALM. (d) HaLRTC. (e) TMac. (f) LRTC-TV. (g) Trace/TV. (h) t-SVD. (i) McpTC. (j) ScadTC. (k) FTNN. (l) TLNM. (m) TLNMTV.

4.1. HSI Completion

The HSI¹ test data is used in the experiment came from the open source CAVE data sets (respectively named "chart_and_stuffed_toy", "cloth", "feathers", "flowers", "beads", "oil_painting"). The size of HSI is $512 \times 512 \times 31$, indicating that the spatial resolution is 512×512 and the spectral resolution is 31, respectively. We show the visual effects of HSI recovery with sampling rates of 5%, 10% and 20%

¹<http://www.cs.columbia.edu/CAVE/databases/multispectral/>

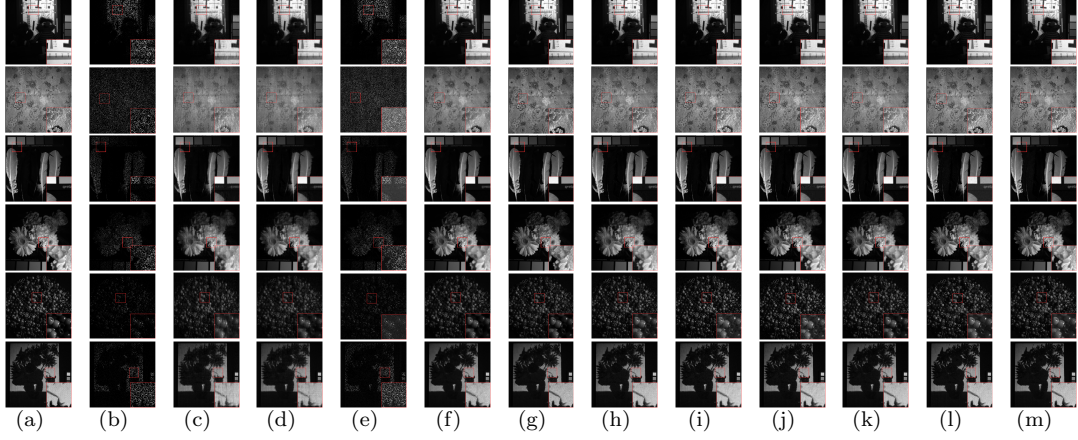


Figure 3: (a) Original images. (b) Corresponding sampled images with SR 20%. (c)-(l) and (m) Completed images achieved by nine competing methods and proposed TLNM method and TLNMTV method, respectively. (a) Original image. (b) Observed image. (c) MC-ALM. (d) HaLRTC. (e) TMac. (f) LRTC-TV. (g) Trace/TV. (h) t-SVD. (i) McpTC. (j) ScadTC. (k) FTNN. (l) TLNM. (m) TLNMTV.

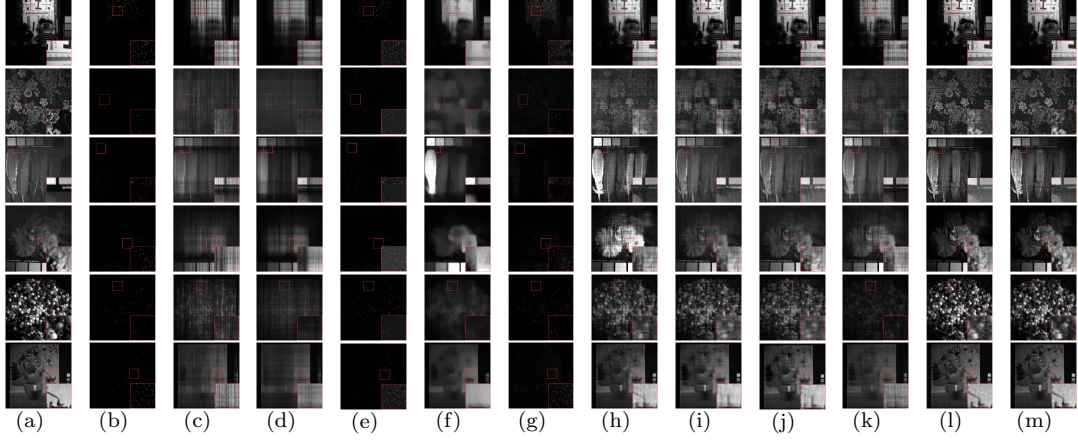
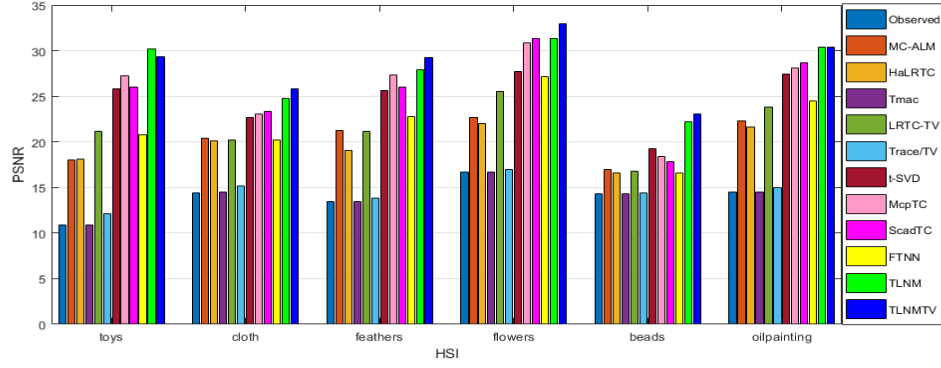
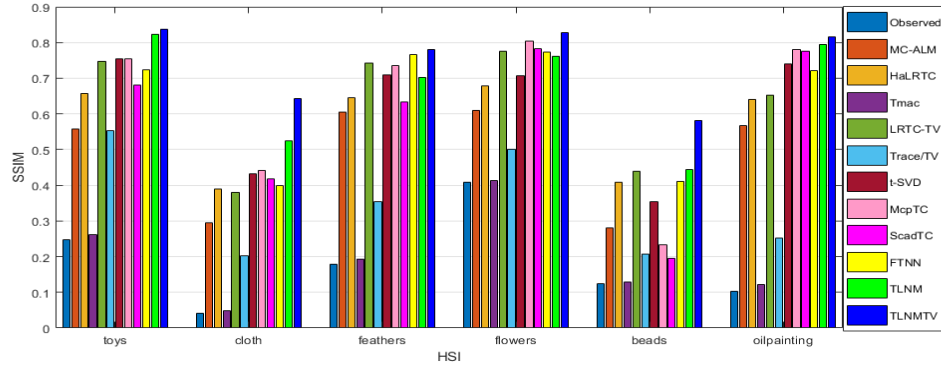


Figure 4: (a) Original images. (b) Corresponding sampled images with SR 2.5%. (c)-(l) and (m) Completed images achieved by nine competing methods and proposed TLNM method and TLNMTV method, respectively. (a) Original image. (b) Observed image. (c) MC-ALM. (d) HaLRTC. (e) TMac. (f) LRTC-TV. (g) Trace/TV. (h) t-SVD. (i) McpTC. (j) ScadTC. (k) FTNN. (l) TLNM. (m) TLNMTV.

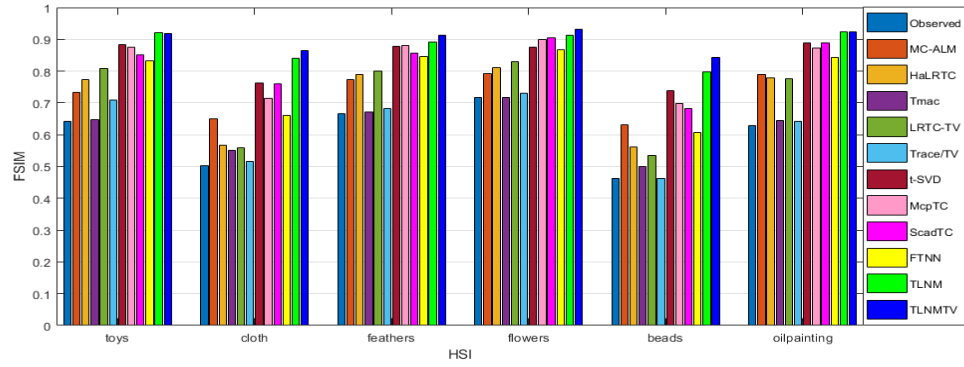
respectively in Figs.1-3, in which the small figure is a local enlargement. It can be seen from the figure that the two proposed methods are superior to other methods, and TLNMTV method is more accurate on the details. Table 1 lists the average quantitative numerical results of HSI at three sampling rates. It is not difficult to find that the proposed TLNM method is far superior to the classical HaLRTC method based on SNN and t-SVD method based on TNN. This shows that the proposed SNN method combined with QR decomposition and $L_{2,1}$ norm can improve the recovery effect. At 5% sampling rate, the PSNR value of TLNMTV method is 3dB higher than that of suboptimal method. Even at



(a)



(b)



(c)

Figure 5: The PSNR, SSIM, and FSIM of the results by different methods on all the HSI data with the sampling rate 2.5%.

20% sampling rate, the TLNMTV method is still 1dB higher than the suboptimal FTNN method.

Through the above experimental study, it is found that our method has a better effect at a lower sampling rate. In view of this, we have done experiments at a sampling rate of 2.5%. Fig. 4 shows the visual effect at a 2.5% sampling rate, and Fig. 5 further illustrates the PSNR, SSIM, and FSIM of all methods on all HSIs. It can be seen from Fig. 4 that our method can still obtain more significant recovery effect at a very low sampling rate of 2.5%, which is quite effective in extracting both global visual and structural information and local detail information. And Fig. 5 shows that when the sampling rate is 2.5%, the results obtained by our method are better than those obtained by other state-of-the-art methods.

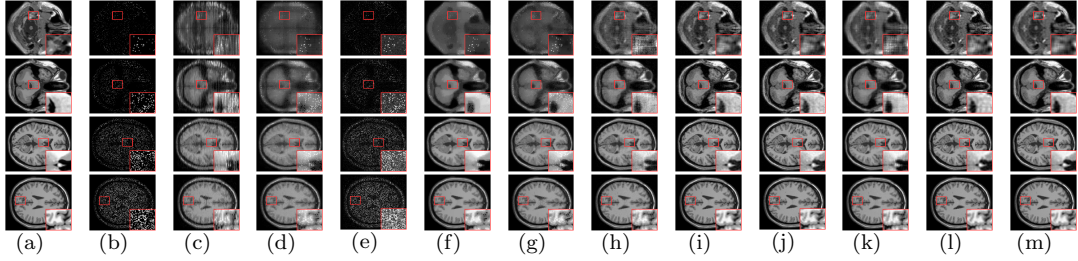


Figure 6: (a) Original images. (b) Corresponding sampled images with SR 5% to 30%. (c)-(l) and (m) Completed images achieved by nine competing methods and proposed TLNM method and TLNMTV method, respectively. (a) Original image. (b) Observed image. (c) MC-ALM. (d) HaLRTC. (e) TMac. (f) LRTC-TV. (g) Trace/TV. (h) t-SVD. (i) McpTC. (j) ScadTC. (k) FTNN. (l) TLNM. (m) TLNMTV.

Table 2: Quantitative evaluation of the results for MRI with different SRs.

SR	index	Observed	MC-ALM	HaLRTC	Tmac	LRTC-TV	Trace-TV	t-SVD	McpTC	ScadTC	FTNN	TLNM	TLNMTV
5%	PSNR	9.908	17.513	16.934	9.951	19.000	18.095	22.720	27.520	27.531	24.164	27.227	27.541
	SSIM	0.174	0.289	0.299	0.103	0.530	0.464	0.514	0.748	0.748	0.653	0.724	0.782
	FSIM	0.457	0.670	0.614	0.553	0.663	0.657	0.770	0.855	0.855	0.819	0.845	0.857
	ERGAS	1025.997	431.950	463.986	1021.063	363.138	414.979	242.057	135.859	135.675	203.091	141.034	135.572
10%	PSNR	10.143	20.171	19.910	10.284	22.579	21.763	25.431	30.154	30.156	27.010	30.330	31.797
	SSIM	0.188	0.452	0.448	0.093	0.712	0.637	0.656	0.830	0.830	0.780	0.846	0.914
	FSIM	0.492	0.746	0.717	0.564	0.787	0.777	0.830	0.895	0.895	0.874	0.897	0.927
	ERGAS	998.616	317.697	328.310	982.744	240.306	270.797	178.582	100.559	100.528	146.333	99.056	83.339
20%	PSNR	10.656	23.458	24.151	11.143	27.659	26.219	29.224	34.587	34.448	30.880	34.130	35.778
	SSIM	0.219	0.640	0.671	0.112	0.874	0.814	0.809	0.937	0.932	0.892	0.936	0.965
	FSIM	0.544	0.824	0.828	0.569	0.899	0.882	0.899	0.953	0.950	0.930	0.946	0.967
	ERGAS	941.393	216.791	200.759	890.839	134.009	162.074	116.642	60.244	61.197	93.371	63.738	52.713
30%	PSNR	11.231	25.921	27.584	11.950	30.867	29.330	32.172	37.987	37.206	33.712	37.591	38.364
	SSIM	0.253	0.760	0.814	0.144	0.932	0.895	0.888	0.977	0.966	0.940	0.972	0.980
	FSIM	0.575	0.875	0.895	0.580	0.944	0.930	0.938	0.979	0.974	0.958	0.975	0.981
	ERGAS	881.074	163.086	134.957	812.918	92.554	113.377	83.475	40.760	44.527	67.186	42.717	39.060

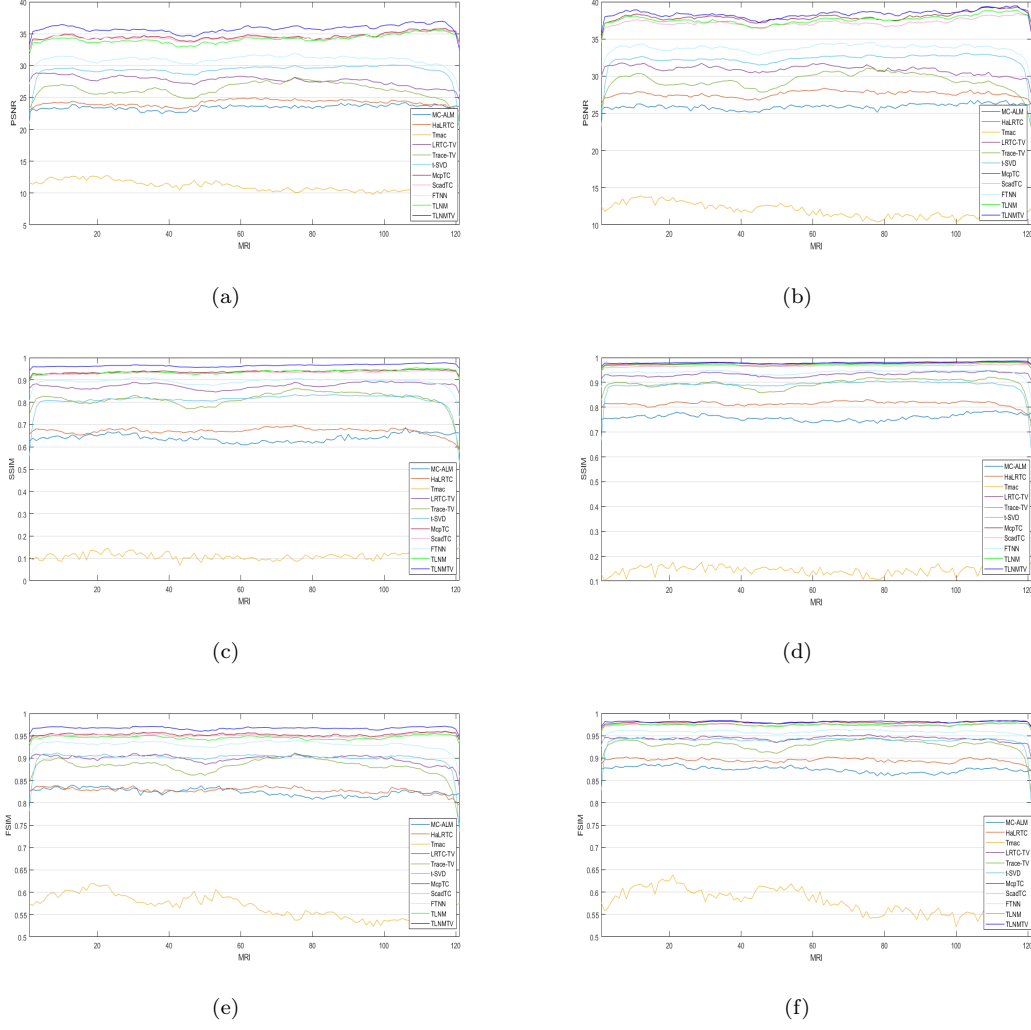


Figure 7: PSNR, SSIM, and FSIM values comparison of different methods for each slice on MRI data sets, (a), (c), (e) under SR 20%, (b), (d), (f) under SR 30%.

4.2. MRI Completion

We test the performance of the proposed method and the comparison method on MRI² data with the size of $181 \times 217 \times 121$. Fig. 6 shows the visual effects of MRI images at the sampling rate of 5%, 10%, 20% and 30% respectively. It can be found from the figure that for the visual effect of MRI image recovery, our method is superior to the comparison method in both global and local information recovery. Further, Fig. 7 describes the specific values of PSNR, SSIM and FSIM of each slice at the sampling rate of 20% and 30%. As one can see from Fig. 7 that the TLNMTV method is the optimal

²http://brainweb.bic.mni.mcgill.ca/brainweb/selection_normal.html

method. Table 2 reports the PSNR, SSIM, FSIM, ERGAS values for each sample rate. It can be seen from the table that at different sampling rates, the TLNM method is obviously superior to the HaLRTC and t-SVD, and the results obtained are very close to those obtained by non-convex method McpTC. Both methods are based on SNN, which indicates that the convex TLNM method is very efficient. In addition, the TLNMTV method is obviously superior to the suboptimal method McpTC. Even when the sampling rate is 20%, the PSNR value of TLNMTV method is 1.2 dB higher than that of McpTC.

5. Parameters setting and Convergency Behaviours

We obtain the optimal solutions of the two algorithm parameters through experimental tests. Table 3 lists the optimal parameters of r_n for different images with different sampling rates. We let α and $\beta = [1/N, 1/N, \dots, 1/N]$. In order to observe the convergence behavior of the algorithm, the relative error (RE) of the recovery tensor is defined as follows:

$$RE := \frac{\|\mathcal{X}_{rec} - \mathcal{X}_o\|_F}{\|\mathcal{X}_o\|_F}, \quad (42)$$

where \mathcal{X}_{rec} is recovery tensor and \mathcal{X}_o is origin tensor. Fig. 8 shows the iterative RE of the proposed algorithm for HSI and MRI. As the iteration progresses, the RE can become smaller, which guarantees the convergence of the proposed algorithm.

Table 3: The value of r_n is set for different images with different SRs.

Method	TLNM				TLNMTV			
SR	2.50%	5%	10%	20%	2.50%	5%	10%	20%
chart and stuffed toy	50 50 4	85 85 4	125 125 4	205 205 4	60 60 4	95 95 4	145 145 4	205 205 4
cloth	50 50 4	85 85 4	125 125 4	205 205 4	130 130 4	160 160 4	235 235 4	275 275 4
feather	40 40 4	65 65 4	105 105 4	205 205 4	50 50 4	95 95 4	145 145 4	205 205 4
flower	50 50 4	75 75 4	125 125 4	205 205 4	50 50 4	95 95 4	165 165 4	205 205 4
beads	50 50 4	115 115 4	175 175 4	255 255 4	110 110 4	155 155 4	215 215 4	235 235 4
oil painting	60 60 4	95 95 4	185 185 4	235 235 4	80 80 4	135 135 4	205 205 4	250 250 4
SR	5%	10%	20%	30%	5%	10%	20%	30%
MRI	50 60 30	60 70 40	70 90 55	90 110 60	50 60 30	80 90 40	100 120 55	110 130 60

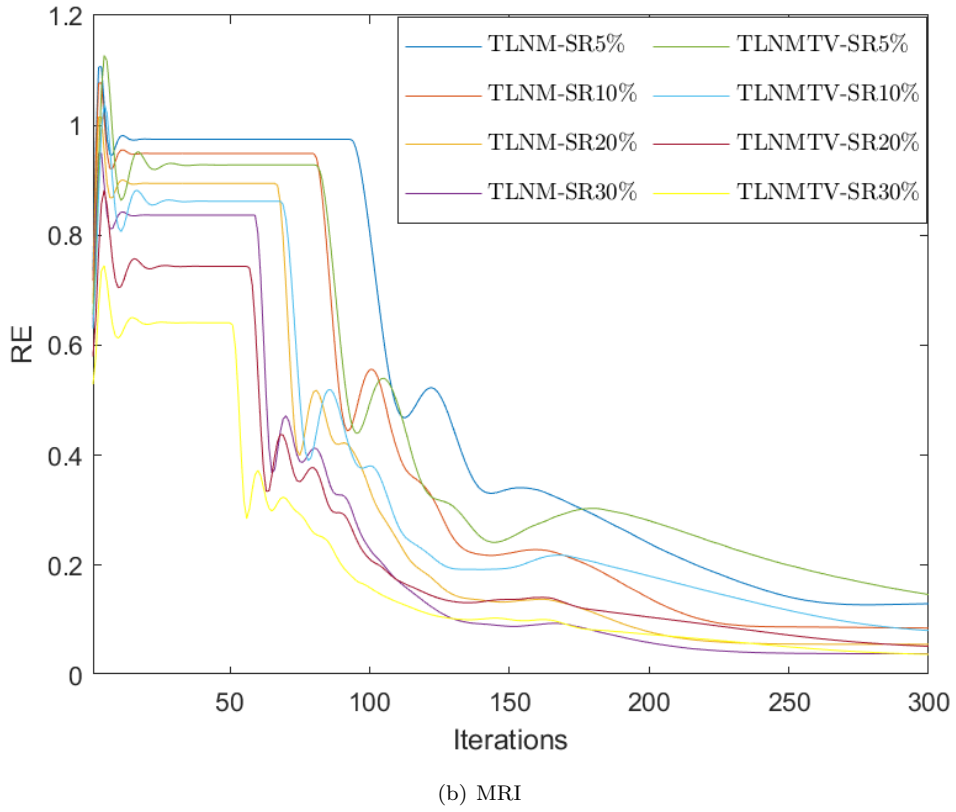
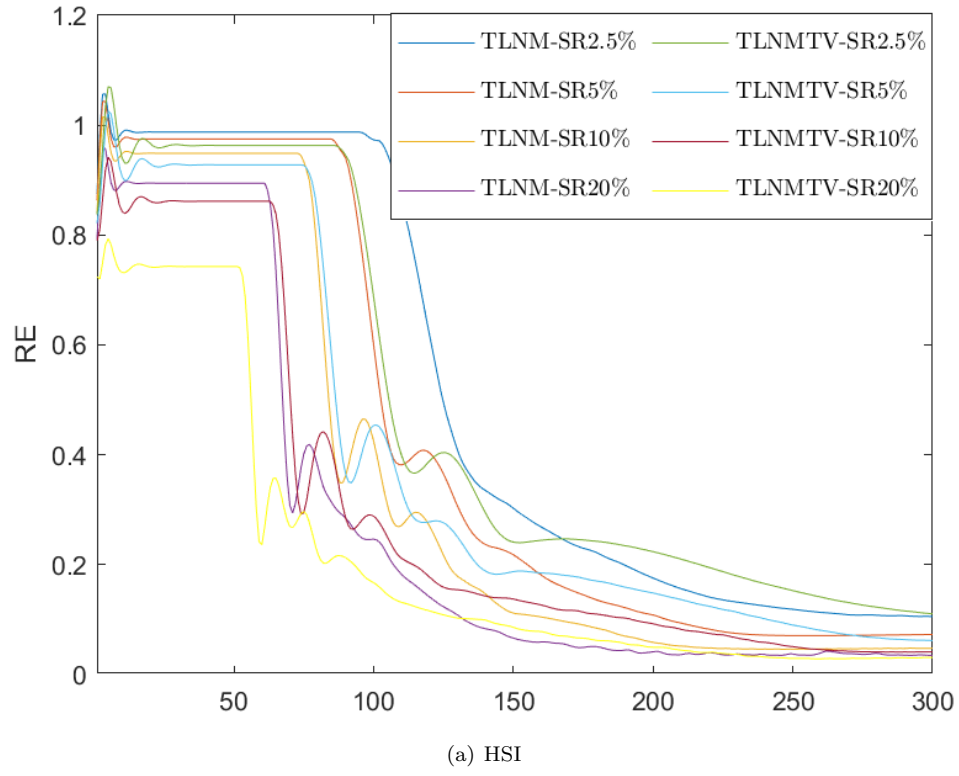


Figure 8: The convergence behaviours of LRTC Algorithm, with respect to different sampling rates.

6. Conclusion

This paper integrates SNN with QR decomposition and $L_{2,1}$ norm to solve the LRTC problem, and proposes the TLNM method. The TV regularization term is further introduced to improve the local prior information and make the recovery effect of the TLNM method more ideal. HSI and MRI are tested at different sampling rates. Experiments show that our TLNM method is more efficient than the TNN-based TLNM-TQR method and outperforms the classic HaLRTC and t-SVD methods. Besides, the TLMNTV method surpasses other compared methods in this paper, thus confirming the high efficiency of our proposed method. It is particularly worth emphasizing that our method still achieves fairly good HSI recovery when the SR is extremely low, i.e. 2.5%. In future work, we will try to introduce other more efficient forms, such as non-convex transformations to replace the nuclear norm, to further improve the recovery performance of our method.

References

- [1] Y.-M. Huang, H.-Y. Yan, Y.-W. Wen, X. Yang, Rank minimization with applications to image noise removal, *Information Sciences* 429 (2018) 147–163.
- [2] B. Madathil, S. N. George, Twist tensor total variation regularized-reweighted nuclear norm based tensor completion for video missing area recovery, *Information Sciences* 423 (2018) 376–397.
- [3] H. Zhang, X. Liu, H. Fan, Y. Li, Y. Ye, Tensor full feature measure and its nonconvex relaxation applications to tensor recovery, *arXiv preprint arXiv:2109.12257* (2021).
- [4] J.-H. Yang, X.-L. Zhao, T.-Y. Ji, T.-H. Ma, T.-Z. Huang, Low-rank tensor train for tensor robust principal component analysis, *Applied Mathematics and Computation* 367 (2020) 124783.
- [5] J. Xue, Y. Zhao, W. Liao, J. Cheung-Wai Chan, Nonconvex tensor rank minimization and its applications to tensor recovery, *Information Sciences* 503 (2019) 109–128. doi:<https://doi.org/10.1016/j.ins.2019.06.061>.
- [6] X. Fu, W.-K. Ma, J. M. Bioucas-Dias, T.-H. Chan, Semiblind hyperspectral unmixing in the presence of spectral library mismatches, *IEEE Transactions on Geoscience and Remote Sensing* 54 (9) (2016) 5171–5184.
- [7] J. Xue, Y. Zhao, W. Liao, J. C.-W. Chan, Nonlocal low-rank regularized tensor decomposition for hyperspectral image denoising, *IEEE Transactions on Geoscience and Remote Sensing* 57 (7) (2019) 5174–5189. doi:[10.1109/TGRS.2019.2897316](https://doi.org/10.1109/TGRS.2019.2897316).

- [8] L. Zhang, L. Zhang, D. Tao, X. Huang, Tensor discriminative locality alignment for hyperspectral image spectral-spatial feature extraction, *IEEE Transactions on Geoscience and Remote Sensing* 51 (1) (2013) 242–256. doi:10.1109/TGRS.2012.2197860.
- [9] Q. Li, D. Schonfeld, Multilinear discriminant analysis for higher-order tensor data classification, *IEEE Transactions on Pattern Analysis and Machine Intelligence* 36 (12) (2014) 2524–2537. doi:10.1109/TPAMI.2014.2342214.
- [10] X. Cao, X. Wei, Y. Han, D. Lin, Robust face clustering via tensor decomposition, *IEEE Transactions on Cybernetics* 45 (11) (2015) 2546–2557. doi:10.1109/TCYB.2014.2376938.
- [11] J. Xue, Y. Zhao, W. Liao, J. C.-W. Chan, S. G. Kong, Enhanced sparsity prior model for low-rank tensor completion, *IEEE Transactions on Neural Networks and Learning Systems* 31 (11) (2020) 4567–4581. doi:10.1109/TNNLS.2019.2956153.
- [12] E. Acar, D. M. Dunlavy, T. G. Kolda, M. Mørup, Scalable tensor factorizations for incomplete data, *Chemometrics and Intelligent Laboratory Systems* 106 (1) (2011) 41–56.
- [13] P. Tichavský, A.-H. Phan, A. Cichocki, Numerical cp decomposition of some difficult tensors, *Journal of Computational and Applied Mathematics* 317 (2017) 362–370.
- [14] R. Harshman, Foundations of the parafac procedure: Model and conditions for an “explanatory” multi-mode factor analysis, *UCLA Work. Pap. Phon.* 16 (11 1969).
- [15] L. Tucker, Some mathematical notes on three-mode factor analysis, *Psychometrika* 31 (1966) 279–311.
- [16] W. Cao, Y. Wang, J. Sun, D. Meng, C. Yang, A. Cichocki, Z. Xu, Total variation regularized tensor rpca for background subtraction from compressive measurements, *IEEE Transactions on Image Processing* 25 (9) (2016) 4075–4090.
- [17] M. E. Kilmer, C. D. Martin, Factorization strategies for third-order tensors, *Linear Algebra and its Applications* 435 (3) (2011) 641–658.
- [18] Z. Zhang, G. Ely, S. Aeron, N. Hao, M. Kilmer, Novel methods for multilinear data completion and de-noising based on tensor-svd, *2014 IEEE Conference on Computer Vision and Pattern Recognition* (2014) 3842–3849.
- [19] C. J. Hillar, L.-H. Lim, Most tensor problems are np-hard, *Journal of the ACM (JACM)* 60 (6) (2013) 1–39.

- [20] Y.-F. Li, K. Shang, Z.-H. Huang, Low tucker rank tensor recovery via admm based on exact and inexact iteratively reweighted algorithms, *Journal of Computational and Applied Mathematics* 331 (2018) 64–81.
- [21] X. Li, M. K. Ng, G. Cong, Y. Ye, Q. Wu, Mr-ntd: Manifold regularization nonnegative tucker decomposition for tensor data dimension reduction and representation, *IEEE Transactions on Neural Networks and Learning Systems* 28 (8) (2017) 1787–1800. doi:10.1109/TNNLS.2016.2545400.
- [22] K. Braman, Third-order tensors as linear operators on a space of matrices, *Linear Algebra and its Applications* 433 (7) (2010) 1241–1253.
- [23] M. E. Kilmer, C. D. Martin, Factorization strategies for third-order tensors, *Linear Algebra and its Applications* 435 (3) (2011) 641–658.
- [24] J. Liu, P. Musialski, P. Wonka, J. Ye, Tensor completion for estimating missing values in visual data, *IEEE Transactions on Pattern Analysis and Machine Intelligence* 35 (1) (2013) 208–220. doi:10.1109/TPAMI.2012.39.
- [25] N. Paragios, Y. Chen, O. Faugeras, *Handbook of Mathematical Models in Computer Vision — Total Variation Image Restoration: Overview and Recent Developments*, Vol. 10.1007/0-387-28831-7, Springer Science & Business Media, 2006.
- [26] X. Cao, L. Yang, X. Guo, Total variation regularized rpca for irregularly moving object detection under dynamic background, *IEEE Transactions on Cybernetics* 46 (4) (2016) 1014–1027. doi:10.1109/TCYB.2015.2419737.
- [27] J. Xue, Y. Zhao, W. Liao, J. Cheung-Wai Chan, Total variation and rank-1 constraint rpca for background subtraction, *IEEE Access* 6 (2018) 49955–49966. doi:10.1109/ACCESS.2018.2868731.
- [28] B. Madathil, S. N. George, Twist tensor total variation regularized-reweighted nuclear norm based tensor completion for video missing area recovery, *Information Sciences* 423 (2018) 376–397.
- [29] H. Wang, F. Nie, H. Huang, Low-rank tensor completion with spatio-temporal consistency, *Proceedings of the Twenty-Eighth AAAI Conference on Artificial Intelligence* 4 (2014) 2846–2852.
- [30] Y. Xu, R. Hao, W. Yin, Z. Su, Parallel matrix factorization for low-rank tensor completion, *Inverse Problems and Imaging* 9 (2015) 601–624. doi:10.3934/ipi.2015.9.601.
- [31] X. Li, Y. Ye, X. Xu, Low-rank tensor completion with total variation for visual data inpainting, *Proceedings of the Thirty-First AAAI Conference on Artificial Intelligence* (2017) 2210–2216.

- [32] X. Guo, Y. Ma, Generalized tensor total variation minimization for visual data recovery?, 2015 IEEE Conference on Computer Vision and Pattern Recognition (CVPR) (2015) 3603–3611.
- [33] Q. Liu, F. Davoine, J. Yang, Y. Cui, Z. Jin, F. Han, A fast and accurate matrix completion method based on qr decomposition and $l_{2,1}$ -norm minimization, IEEE Transactions on Neural Networks and Learning Systems 30 (3) (2019) 803–817.
- [34] Y. Zheng, A.-B. Xu, Tensor completion via tensor qr decomposition and $l_{2,1}$ -norm minimization, Signal Processing 189 (2021) 108240.
- [35] S. Boyd, N. Parikh, E. Chu, Distributed optimization and statistical learning via the alternating direction method of multipliers, Now Publishers Inc, 2011.
- [36] Z. Lin, R. Liu, Z. Su, Linearized alternating direction method with adaptive penalty for low-rank representation, Advances in Neural Information Processing Systems 24 (2011) 612–620.
- [37] T. G. Kolda, B. W. Bader, Tensor decompositions and applications, SIAM review 51 (3) (2009) 455–500.
- [38] G. Liu, Z. Lin, Y. Yu, Robust subspace segmentation by low-rank representation, ICML 2010 - Proceedings, 27th International Conference on Machine Learning (2010) 663–670.
- [39] Z. Wang, A. Bovik, H. Sheikh, E. Simoncelli, Image quality assessment: from error visibility to structural similarity, IEEE Transactions on Image Processing 13 (4) (2004) 600–612. doi:10.1109/TIP.2003.819861.
- [40] L. Zhang, L. Zhang, X. Mou, D. Zhang, Fsim: A feature similarity index for image quality assessment, IEEE Transactions on Image Processing 20 (8) (2011) 2378–2386. doi:10.1109/TIP.2011.2109730.
- [41] L. Wald, Data fusion: definitions and architectures: fusion of images of different spatial resolutions, Presses des MINES, 2002.
- [42] Z. Zhang, S. Aeron, Exact tensor completion using t-svd, IEEE Transactions on Signal Processing 65 (6) (2017) 1511–1526. doi:10.1109/TSP.2016.2639466.
- [43] Z. Lin, M. Chen, Y. Ma, The augmented lagrange multiplier method for exact recovery of corrupted low-rank matrices, Mathematical Programming 9 (09 2010).
- [44] W. Cao, Y. Wang, C. Yang, X. Chang, Z. Han, Z. Xu, Folded-concave penalization approaches to tensor completion, Neurocomputing 152 (2015) 261–273.

- [45] T.-X. Jiang, M. K. Ng, X.-L. Zhao, T.-Z. Huang, Framelet representation of tensor nuclear norm for third-order tensor completion, *IEEE Transactions on Image Processing* 29 (2020) 7233–7244. doi:10.1109/TIP.2020.3000349.
- [46] M. M, H. LK, A. SM, Algorithms for sparse nonnegative tucker decompositions, *Neural computation* 20 (8) (2008) 2112–2131.